Branch Voltage Balancing Control Strategy Based on the Transfer Power Model by Zero-Sequence Circulating Current for the Hexverter

YANG YI[ID], GANG YANG, CHONG QIAN, AND YAOJIE GUI

Fujian Key Laboratory of New Energy Generation and Power Conversion, Fuzhou University, Fuzhou 350108, China

Corresponding author: Yang Yi (yiyang@fzu.edu.cn)

ABSTRACT This paper proposes a novel branch voltage-balancing control strategy for a hexagonal converter (Hexverter). First, the state-space model based on the double-dq transformation is analyzed in-depth along with the necessary basic mathematical derivation, and the active/reactive power control model in the dq reference frame for the Hexverter is proposed. Second, a zero-sequence double-loop network consisting of a Y-loop and a Hex-loop circulating current was established. This study proposes a method to suppress the Y-loop circulating current by connecting a capacitor at the neutral point. We then establish a novel branch voltage-balancing control strategy based on the transfer power model. The essence of the proposed control strategy is to control the charging and discharging states of each submodule via the zero-sequence voltages and the Hex-loop circulating current to regulate the power transfer between adjacent submodules and branches, thereby effectively ensuring the dynamic balance of the DC voltages of the submodules. The branch voltage-balancing control model and power control model proposed in this paper are based on zero-sequence and positive-sequence networks, respectively. The relative independence of the positive- and zero-sequence networks leads to decoupling of the branch voltage-balancing control model and the power control model; thus, the respective control objectives can be achieved by adjusting the respective control variables independently. It has a stronger adaptability to diverse power grid operating parameters. Finally, the validity and correctness of the mathematical model and control strategy proposed in this study are verified using MATLAB/Simulink.

INDEX TERMS Hexverter, double-dq transformation, the zero-sequence double-loop network, the transfer power model, the voltage balancing control, circulating current suppression.

I. INTRODUCTION

The AC-AC converter is a family of power electronic topologies that can connect two AC systems of different frequencies directly without a central DC link [1], [2]. It is suitable for use in fractional-frequency transmission systems (FFTS), multifrequency power systems, high-power low-speed motor drives, asynchronous power system interconnections, and other scenarios.

A modular multilevel matrix converter(M3C) [3]–[5] is a typical AC-AC converter. M3C requires nine branches to achieve power conversion, and each branch is cascaded by several full-bridge submodules. Therefore, the topology leads to a larger volume and a higher cost. In addition, M3C has numerous circulating current paths, which complicate the circulating current analysis and suppression control.

Based on M3C, a particular topology named the hexagonal converter (Hexverter) was proposed in [6]. Compared with M3C, the number of branches was reduced from nine to six, and the volume and cost were also significantly reduced. In addition, Hexverter has only one circulating current path, which simplifies the circulating current analysis and suppression control. Therefore, Hexverter has great potential for various applications.

In the last two decades, many scholars have focused on their operating principles and control-oriented models,

---

The associate editor coordinating the review of this manuscript and approving it for publication was S. K. Panda[ID].

as well as the necessary mathematical analysis. The electrical characteristics and control strategy of Hexverter are obtained. In [7], the authors developed a state-space model of Hexverter in the $\alpha\beta$ frame and verified its operating characteristics using an experimental prototype. In [8]–[10], based on the state-space model, a frequency-decoupled branch current control model in the dq reference frame was presented, and the operating principle and characteristic waveforms were verified with a simulation and experimental prototype. To solve the problems of difficulty in tuning proportional-integral (PI) parameters to ensure global stability, a global asymptotical stable control scheme of Hexverter based on the IDA-PBC methodology was presented in [11].

According to the characteristic analysis of branch power [6], [12], the branch power differs between adjacent branches depending on the difference between the reactive powers in both systems. The branch power differs leads to a significant imbalance of adjacent branches and further results in a system breakdown or insufficient branch voltage reserves for the control system. Moreover, differences in DC capacitor losses, switching losses, and PWM asymmetry will cause a slight imbalance between the DC voltages of each submodule. Therefore, branch voltage-balancing control and circulating current suppression control are important for the steady-state operation of the Hexverter. Regulating the modulation ratio in a small range is a conventional method to realize voltage balancing for multilevel converters [11]. Compensating for branch power differs by superimposing common-mode voltages on the neutral points, and injecting circulating current is another solution to this problem [13], [14].

The branch power differs significantly when the difference between the reactive powers in both systems is significant. Compensation for significant power differs requires a wide range of modulation-ratio adjustments. This affects the control performance of active and reactive power and makes the tuning of proportional-integral (PI) parameters difficult. Moreover, the topology and grounding method jointly determine the circulating current path of Hexverter. A typical power system has multiple grounding points, which provide numerous circulating current paths. This complicates the circulating current analysis for Hexverter. Circulating currents in different paths have different characteristics and should be analyzed separately. However, none of the previous studies has addressed these problems.

In this study, a novel branch voltage-balancing control strategy was proposed. First, based on the state-space model, a control strategy in a double-dq frame for Hexverter was proposed [15]. It realizes flexible active/reactive power control on both sides and achieves overall stability of the stored energy. Second, a novel branch voltage-balancing control strategy based on the transfer power model was established. Based on the control strategy, the transfer power among adjacent branches can be regulated by the zero-sequence voltages and Hex-loop circulating current, and it is performed to effectively ensure the dynamic balance of submodules DC voltages. Finally, the validity and correctness of the mathematical

model and control strategy proposed in this study are verified using MATLAB/Simulink.

The remainder of this paper is organized as follows. In Section II, the operating principle of Hexverter is described, and the double-dq transformation based on the state-space model is analyzed in depth along with the necessary basic mathematical derivation. In Section III, the control scheme of Hexverter is described, including a novel branch voltage-balancing control strategy based on the transfer power model. Section IV describes the construction of a simulation model of the asynchronous power system interconnection based on Hexverter using MATLAB/Simulink. This verifies the feasibility of Hexverter and the effectiveness of the control scheme proposed in this study.

II. PRINCIPLE OF OPERATION

A. TOPOLOGY OF THE HEXVERTER

The Hexverter topology is illustrated in Fig. 1. Hexverter consists of six identical branches that formed a hexagonal ring. Each branch is cascaded by n identical full-bridge submodules and branch inductances. Hexverter directly connects two three-phase systems. The two three-phase systems are alternately connected to the connection points of the branches [15].
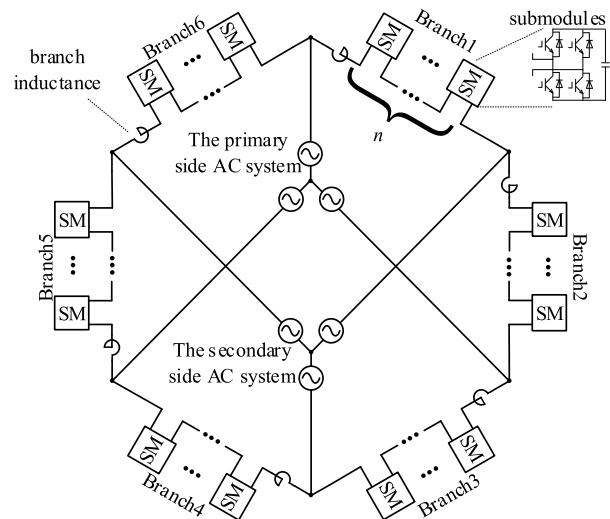

FIGURE 1. Hexverter topology.

B. BASIC MATHEMATICAL MODEL

1) VOLTAGES TRANSFORMATION

The equivalent circuit of Hexverter is illustrated in Fig. 2. The submodules in each branch are replaced by a variable voltage source u_j with $j \in \{1, 2, 3, 4, 5, 6\}$ in series with the branch inductance l and equivalent internal resistance r. The branch currents are i_j with $j \in \{1, 2, 3, 4, 5, 6\}$. The voltages and currents of the primary-side AC system are u_{pj} with $j \in \{a, b, c\}$ and i_{pj} with $j \in \{a, b, c\}$, and those of the secondary-side AC system are u_{sj} with $j \in \{a, b, c\}$ and i_{sj} with $j \in \{a, b, c\}$. The voltage between the neutral points of the two systems is u_{nN}.

According to the Kirchhoff voltage law (KVL), the state-space equations of Hexverter can be determined from Fig.2.

$$
\begin{bmatrix} u_{pa} \\ u_{pb} \\ u_{pc} \end{bmatrix} = -r \begin{bmatrix} i_1 \\ i_3 \\ i_5 \end{bmatrix} - l \frac{d}{dt} \begin{bmatrix} i_1 \\ i_3 \\ i_5 \end{bmatrix} + \begin{bmatrix} u_1 \\ u_3 \\ u_5 \end{bmatrix} + \begin{bmatrix} u_{sa} \\ u_{sb} \\ u_{sc} \end{bmatrix}
$$

$$
+ \begin{bmatrix} u_{nN} \\ u_{nN} \\ u_{nN} \end{bmatrix} \tag{1}
$$

$$
\begin{bmatrix} u_{sa} \\ u_{sb} \\ u_{sc} \end{bmatrix} = -r \begin{bmatrix} i_2 \\ i_4 \\ i_6 \end{bmatrix} - l \frac{d}{dt} \begin{bmatrix} i_2 \\ i_4 \\ i_6 \end{bmatrix} + \begin{bmatrix} u_2 \\ u_4 \\ u_6 \end{bmatrix} + \begin{bmatrix} u_{pb} \\ u_{pc} \\ u_{pa} \end{bmatrix}
$$

$$
- \begin{bmatrix} u_{nN} \\ u_{nN} \\ u_{nN} \end{bmatrix} \tag{2}
$$

Both branch voltages and currents contain two frequency components for both systems [6]. The subscripts -fp and -fs represent the primary-and secondary-side frequency components of the variables, respectively. The frequency-decoupled voltage equations of (1) are obtained in (3):

$$
\begin{cases}
\begin{bmatrix} u_{pa} \\ u_{pb} \\ u_{pc} \end{bmatrix} = -r \begin{bmatrix} i_{1\text{-fp}} \\ i_{3\text{-fp}} \\ i_{5\text{-fp}} \end{bmatrix} - l \frac{d}{dt} \begin{bmatrix} i_{1\text{-fp}} \\ i_{3\text{-fp}} \\ i_{5\text{-fp}} \end{bmatrix} + \begin{bmatrix} u_{1\text{-fp}} \\ u_{3\text{-fp}} \\ u_{5\text{-fp}} \end{bmatrix} \\
\qquad + \begin{bmatrix} u_{nN} \\ u_{nN} \\ u_{nN} \end{bmatrix} \\
0 = -r \begin{bmatrix} i_{1\text{-fs}} \\ i_{3\text{-fs}} \\ i_{5\text{-fs}} \end{bmatrix} - l \frac{d}{dt} \begin{bmatrix} i_{1\text{-fs}} \\ i_{3\text{-fs}} \\ i_{5\text{-fs}} \end{bmatrix} + \begin{bmatrix} u_{1\text{-fs}} \\ u_{3\text{-fs}} \\ u_{5\text{-fs}} \end{bmatrix} + \begin{bmatrix} u_{sa} \\ u_{sb} \\ u_{sc} \end{bmatrix} \\
\qquad + \begin{bmatrix} u_{nN} \\ u_{nN} \\ u_{nN} \end{bmatrix}
\end{cases} \tag{3}
$$

Apply *dq* transformation to (3). All the variables in (3) are *dq*-transformed at the frequencies of each AC system, and the voltage equations of branches {1, 3, 5} in the *dq*0 reference frame are obtained as follows:

$$
\begin{cases}
\begin{bmatrix} u_{xd\text{-fp}} \\ u_{xq\text{-fp}} \\ u_{x0\text{-fp}} \end{bmatrix} = r \begin{bmatrix} i_{xd\text{-fp}} \\ i_{xq\text{-fp}} \\ i_{x0\text{-fp}} \end{bmatrix} + l \frac{d}{dt} \begin{bmatrix} i_{xd\text{-fp}} \\ i_{xq\text{-fp}} \\ i_{x0\text{-fp}} \end{bmatrix} \\
\qquad + l\omega_p \begin{bmatrix} -i_{xq\text{-fp}} \\ i_{xd\text{-fp}} \\ 0 \end{bmatrix} + \begin{bmatrix} u_{pd} \\ u_{pq} \\ u_{p0} \end{bmatrix} - \begin{bmatrix} 0 \\ 0 \\ \sqrt{3}\, u_{nN} \end{bmatrix} \\
\begin{bmatrix} u_{xd\text{-fs}} \\ u_{xq\text{-fs}} \\ u_{x0\text{-fs}} \end{bmatrix} = r \begin{bmatrix} i_{xd\text{-fs}} \\ i_{xq\text{-fs}} \\ i_{x0\text{-fs}} \end{bmatrix} + l \frac{d}{dt} \begin{bmatrix} i_{xd\text{-fs}} \\ i_{xq\text{-fs}} \\ i_{x0\text{-fs}} \end{bmatrix} \\
\qquad + l\omega_s \begin{bmatrix} -i_{xq\text{-fs}} \\ i_{xd\text{-fs}} \\ 0 \end{bmatrix} - \begin{bmatrix} u_{sd} \\ u_{sq} \\ u_{s0} \end{bmatrix} - \begin{bmatrix} 0 \\ 0 \\ \sqrt{3}\, u_{nN} \end{bmatrix}
\end{cases} \tag{4}
$$

where $\{i_{xd\text{-fp}}, i_{xq\text{-fp}}, i_{x0\text{-fp}}\}$ indicates the *dq*0 current components of $\{i_{1\text{-fp}}, i_{3\text{-fp}}, i_{5\text{-fp}}\}$ at the frequency of the primary-side AC system. Similarly, $\{i_{xd\text{-fs}}, i_{xq\text{-fs}}, i_{x0\text{-fs}}\}$ represent the *dq*0 current components of $\{i_{1\text{-fs}}, i_{3\text{-fs}}, i_{5\text{-fs}}\}$ at the frequency of the secondary AC system.

The double-*dq* transformation matrices are defined by:

$$
\begin{cases}
C_p = \sqrt{\frac{2}{3}} \begin{bmatrix} \sin(X_p) & \sin\left(X_p - \frac{2}{3}\pi\right) & \sin\left(X_p + \frac{2}{3}\pi\right) \\ \cos(X_p) & \cos\left(X_p - \frac{2}{3}\pi\right) & \cos\left(X_p + \frac{2}{3}\pi\right) \\ \frac{1}{\sqrt{2}} & \frac{1}{\sqrt{2}} & \frac{1}{\sqrt{2}} \end{bmatrix} \\
C_s = \sqrt{\frac{2}{3}} \begin{bmatrix} \sin(X_s) & \sin\left(X_s - \frac{2}{3}\pi\right) & \sin\left(X_s + \frac{2}{3}\pi\right) \\ \cos(X_s) & \cos\left(X_s - \frac{2}{3}\pi\right) & \cos\left(X_s + \frac{2}{3}\pi\right) \\ \frac{1}{\sqrt{2}} & \frac{1}{\sqrt{2}} & \frac{1}{\sqrt{2}} \end{bmatrix}
\end{cases} \tag{5}
$$

where $X_p = \omega_p t$, $X_s = \omega_s t + \varphi_{ps}$. In addition, ω_p and ω_s are the angular frequencies of the AC system. φ_{ps} represents the phase difference between two AC systems.

According to (2), the state-space equations of branches {2, 4, 6} in the *dq*0 reference frame are obtained as follows:

$$
\begin{cases}
\begin{bmatrix} u_{yd\text{-fp}} \\ u_{yq\text{-fp}} \\ u_{y0\text{-fp}} \end{bmatrix} = r \begin{bmatrix} i_{yd\text{-fp}} \\ i_{yq\text{-fp}} \\ i_{y0\text{-fp}} \end{bmatrix} + l \frac{d}{dt} \begin{bmatrix} i_{yd\text{-fp}} \\ i_{yq\text{-fp}} \\ i_{y0\text{-fp}} \end{bmatrix} \\
\qquad + l\omega_p \begin{bmatrix} -i_{yq\text{-fp}} \\ i_{yd\text{-fp}} \\ 0 \end{bmatrix} - B_p \begin{bmatrix} u_{pd} \\ u_{pq} \\ u_{p0} \end{bmatrix} + \begin{bmatrix} 0 \\ 0 \\ \sqrt{3}\, u_{nN} \end{bmatrix} \\
\begin{bmatrix} u_{yd\text{-fs}} \\ u_{yq\text{-fs}} \\ u_{y0\text{-fs}} \end{bmatrix} = r \begin{bmatrix} i_{yd\text{-fs}} \\ i_{yq\text{-fs}} \\ i_{y0\text{-fs}} \end{bmatrix} + l \frac{d}{dt} \begin{bmatrix} i_{yd\text{-fs}} \\ i_{yq\text{-fs}} \\ i_{y0\text{-fs}} \end{bmatrix} \\
\qquad + l\omega_s \begin{bmatrix} -i_{yq\text{-fs}} \\ i_{yd\text{-fs}} \\ 0 \end{bmatrix} + \begin{bmatrix} u_{sd} \\ u_{sq} \\ u_{s0} \end{bmatrix} + \begin{bmatrix} 0 \\ 0 \\ \sqrt{3}\, u_{nN} \end{bmatrix}
\end{cases} \tag{6}
$$

where $\{i_{yd\text{-fp}}, i_{yq\text{-fp}}, i_{y0\text{-fp}}\}$ indicates the *dq*0 current components of $\{i_{2\text{-fp}}, i_{4\text{-fp}}, i_{6\text{-fp}}\}$ at the frequency of the primary-side AC system. Similarly, $\{i_{yd\text{-fs}}, i_{yq\text{-fs}}, i_{y0\text{-fs}}\}$ indicate the *dq*0 current components of $\{i_{2\text{-fs}}, i_{4\text{-fs}}, i_{6\text{-fs}}\}$ at the frequency of the secondary AC system. The additional matrix B_p is defined as follows:

$$
B_p = C_p \begin{bmatrix} 0 & 1 & 0 \\ 0 & 0 & 1 \\ 1 & 0 & 0 \end{bmatrix} C_p^{-1} \tag{7}
$$

According to (4) and (6), the state-space equations of the branch voltages in the dq reference frame are expressed as

$$
\begin{cases}
\begin{bmatrix} u_{xd\text{-fp}} \\ u_{xq\text{-fp}} \end{bmatrix} = \begin{bmatrix} l\text{p}+r & -l\omega_\text{p} \\ l\omega_\text{p} & l\text{p}+r \end{bmatrix} \begin{bmatrix} i_{xd\text{-fp}} \\ i_{xq\text{-fp}} \end{bmatrix} + \begin{bmatrix} u_{pd} \\ u_{pq} \end{bmatrix} \\[12pt]
\begin{bmatrix} u_{xd\text{-fs}} \\ u_{xq\text{-fs}} \end{bmatrix} = \begin{bmatrix} l\text{p}+r & -l\omega_\text{s} \\ l\omega_\text{s} & l\text{p}+r \end{bmatrix} \begin{bmatrix} i_{xd\text{-fs}} \\ i_{xq\text{-fs}} \end{bmatrix} - \begin{bmatrix} u_{sd} \\ u_{sq} \end{bmatrix} \\[12pt]
\begin{bmatrix} u_{yd\text{-fp}} \\ u_{yq\text{-fp}} \end{bmatrix} = \begin{bmatrix} l\text{p}+r & -l\omega_\text{p} \\ l\omega_\text{p} & l\text{p}+r \end{bmatrix} \begin{bmatrix} i_{yd\text{-fp}} \\ i_{yq\text{-fp}} \end{bmatrix} - B'_\text{p} \begin{bmatrix} u_{pd} \\ u_{pq} \end{bmatrix} \\[12pt]
\begin{bmatrix} u_{yd\text{-fs}} \\ u_{yq\text{-fs}} \end{bmatrix} = \begin{bmatrix} l\text{p}+r & -l\omega_\text{s} \\ l\omega_\text{s} & l\text{p}+r \end{bmatrix} \begin{bmatrix} i_{yd\text{-fs}} \\ i_{yq\text{-fs}} \end{bmatrix} + \begin{bmatrix} u_{sd} \\ u_{sq} \end{bmatrix}
\end{cases}
\tag{8}
$$

where $\text{p} = \text{d/dt}$ denotes the differential operator. The additional matrix B'_p is the upper-left 2×2 matrix of the B_p.

2) CURRENTS TRANSFORMATION

According to Kirchhoff circuit laws (KCL), the state–space equations of Hexverter can be determined from Fig. 2.

$$
\begin{bmatrix} i_{pa} \\ i_{pb} \\ i_{pc} \end{bmatrix} = - \begin{bmatrix} i_1 \\ i_3 \\ i_5 \end{bmatrix} + \begin{bmatrix} i_6 \\ i_2 \\ i_4 \end{bmatrix}
\tag{9}
$$

$$
\begin{bmatrix} i_{sa} \\ i_{sb} \\ i_{sc} \end{bmatrix} = + \begin{bmatrix} i_1 \\ i_3 \\ i_5 \end{bmatrix} - \begin{bmatrix} i_2 \\ i_4 \\ i_6 \end{bmatrix}
\tag{10}
$$

The frequency-decoupled current equations of (9) are obtained in (11):

$$
\begin{cases}
\begin{bmatrix} i_{pa\text{-fp}} \\ i_{pb\text{-fp}} \\ i_{pc\text{-fp}} \end{bmatrix} = - \begin{bmatrix} i_{1\text{-fp}} \\ i_{3\text{-fp}} \\ i_{5\text{-fp}} \end{bmatrix} + \begin{bmatrix} i_{6\text{-fp}} \\ i_{2\text{-fp}} \\ i_{4\text{-fp}} \end{bmatrix} \\[12pt]
\begin{bmatrix} i_{pa\text{-fs}} \\ i_{pb\text{-fs}} \\ i_{pc\text{-fs}} \end{bmatrix} = - \begin{bmatrix} i_{1\text{-fs}} \\ i_{3\text{-fs}} \\ i_{5\text{-fs}} \end{bmatrix} + \begin{bmatrix} i_{6\text{-fs}} \\ i_{2\text{-fs}} \\ i_{4\text{-fs}} \end{bmatrix}
\end{cases}
\tag{11}
$$

All variables in (11) are dq-transformed at the frequencies of each AC system, and the current equations of the primary-side AC system in the $dq0$ reference frame are obtained as follows:

$$
\begin{cases}
\begin{bmatrix} i_{pd\text{-fp}} \\ i_{pq\text{-fp}} \\ i_{p0\text{-fp}} \end{bmatrix} = - \begin{bmatrix} i_{xd\text{-fp}} \\ i_{xq\text{-fp}} \\ i_{x0\text{-fp}} \end{bmatrix} + D_\text{p} \begin{bmatrix} i_{yd\text{-fp}} \\ i_{yq\text{-fp}} \\ i_{y0\text{-fp}} \end{bmatrix} \\[12pt]
\begin{bmatrix} i_{pd\text{-fs}} \\ i_{pq\text{-fs}} \\ i_{p0\text{-fs}} \end{bmatrix} = - \begin{bmatrix} i_{xd\text{-fs}} \\ i_{xq\text{-fs}} \\ i_{x0\text{-fs}} \end{bmatrix} + D_\text{s} \begin{bmatrix} i_{yd\text{-fs}} \\ i_{yq\text{-fs}} \\ i_{y0\text{-fs}} \end{bmatrix}
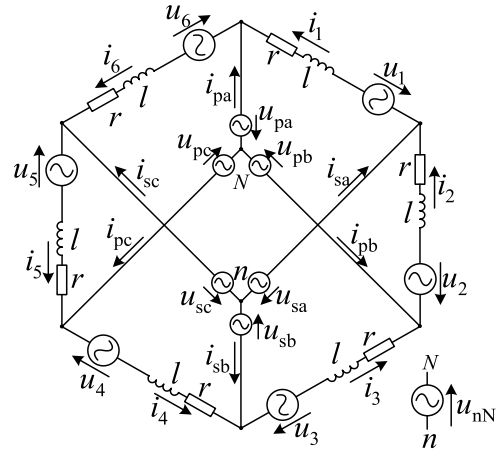\end{cases}
\tag{12}
$$

FIGURE 2. Equivalent circuit of the Hexverter topology.

where the additional matrix D_p and D_s are defined by:

$$
\begin{cases}
D_\text{p} = C_\text{p} \begin{bmatrix} 0 & 0 & 1 \\ 1 & 0 & 0 \\ 0 & 1 & 0 \end{bmatrix} C_\text{p}^{-1} \\[18pt]
D_\text{s} = C_\text{s} \begin{bmatrix} 0 & 0 & 1 \\ 1 & 0 & 0 \\ 0 & 1 & 0 \end{bmatrix} C_\text{s}^{-1}
\end{cases}
\tag{13}
$$

According to Equation (10), the state-space equations of the secondary-side AC system in the $dq0$ reference frame are obtained as follows:

$$
\begin{cases}
\begin{bmatrix} i_{sd\text{-fp}} \\ i_{sq\text{-fp}} \\ i_{s0\text{-fp}} \end{bmatrix} = + \begin{bmatrix} i_{xd\text{-fp}} \\ i_{xq\text{-fp}} \\ i_{x0\text{-fp}} \end{bmatrix} - \begin{bmatrix} i_{yd\text{-fp}} \\ i_{yq\text{-fp}} \\ i_{y0\text{-fp}} \end{bmatrix} \\[12pt]
\begin{bmatrix} i_{sd\text{-fs}} \\ i_{sq\text{-fs}} \\ i_{s0\text{-fs}} \end{bmatrix} = + \begin{bmatrix} i_{xd\text{-fs}} \\ i_{xq\text{-fs}} \\ i_{x0\text{-fs}} \end{bmatrix} - \begin{bmatrix} i_{yd\text{-fs}} \\ i_{yq\text{-fs}} \\ i_{y0\text{-fs}} \end{bmatrix}
\end{cases}
\tag{14}
$$

Substituting (12) into (14), the state-space equations of the branch currents in the $dq0$ reference frame can be expressed as:

$$
\begin{cases}
\begin{bmatrix} i_{yd\text{-fp}} \\ i_{yq\text{-fp}} \\ i_{y0\text{-fp}} \end{bmatrix} = (D_\text{p} - 1)^{-1} \left(\begin{bmatrix} i_{pd\text{-fp}} \\ i_{pq\text{-fp}} \\ i_{p0\text{-fp}} \end{bmatrix} + \begin{bmatrix} i_{sd\text{-fp}} \\ i_{sq\text{-fp}} \\ i_{s0\text{-fp}} \end{bmatrix} \right) \\[18pt]
\begin{bmatrix} i_{yd\text{-fs}} \\ i_{yq\text{-fs}} \\ i_{y0\text{-fs}} \end{bmatrix} = (D_\text{s} - 1)^{-1} \left(\begin{bmatrix} i_{pd\text{-fs}} \\ i_{pq\text{-fs}} \\ i_{p0\text{-fs}} \end{bmatrix} + \begin{bmatrix} i_{sd\text{-fs}} \\ i_{sq\text{-fs}} \\ i_{s0\text{-fs}} \end{bmatrix} \right) \\[18pt]
\begin{bmatrix} i_{xd\text{-fp}} \\ i_{xq\text{-fp}} \\ i_{x0\text{-fp}} \end{bmatrix} = (D_\text{p} - 1)^{-1} \left(\begin{bmatrix} i_{pd\text{-fp}} \\ i_{pq\text{-fp}} \\ i_{p0\text{-fp}} \end{bmatrix} + D_\text{p} \begin{bmatrix} i_{sd\text{-fp}} \\ i_{sq\text{-fp}} \\ i_{s0\text{-fp}} \end{bmatrix} \right) \\[18pt]
\begin{bmatrix} i_{xd\text{-fs}} \\ i_{xq\text{-fs}} \\ i_{x0\text{-fs}} \end{bmatrix} = (D_\text{s} - 1)^{-1} \left(\begin{bmatrix} i_{pd\text{-fs}} \\ i_{pq\text{-fs}} \\ i_{p0\text{-fs}} \end{bmatrix} + D_\text{s} \begin{bmatrix} i_{sd\text{-fs}} \\ i_{sq\text{-fs}} \\ i_{s0\text{-fs}} \end{bmatrix} \right)
\end{cases}
\tag{15}
$$

Equations (8) and (15) are the derivations of the frequency-decoupled state-space equations of the branch voltages and currents in *dq* coordinates and can be obtained as follows:

$$
\begin{cases}
(D_\mathrm{p} - 1) \begin{bmatrix} u_{xd\text{-fp}} \\ u_{xq\text{-fp}} \end{bmatrix} = \begin{bmatrix} l\mathrm{p} + r & -l\omega_\mathrm{p} \\ l\omega_\mathrm{p} & l\mathrm{p} + r \end{bmatrix} \begin{bmatrix} i_{pd\text{-fp}} \\ i_{pq\text{-fp}} \end{bmatrix} \\
\qquad\qquad + (D_\mathrm{p} - 1) \begin{bmatrix} u_{pd} \\ u_{pq} \end{bmatrix} \\
D_\mathrm{s}^{-1}(D_\mathrm{s} - 1) \begin{bmatrix} u_{xd\text{-fs}} \\ u_{xq\text{-fs}} \end{bmatrix} = \begin{bmatrix} l\mathrm{p} + r & -l\omega_\mathrm{s} \\ l\omega_\mathrm{s} & l\mathrm{p} + r \end{bmatrix} \begin{bmatrix} i_{sd\text{-fs}} \\ i_{sq\text{-fs}} \end{bmatrix} \\
\qquad\qquad - D_\mathrm{s}^{-1}(D_\mathrm{s} - 1) \begin{bmatrix} u_{sd} \\ u_{sq} \end{bmatrix} \\
(D_\mathrm{p} - 1) \begin{bmatrix} u_{yd\text{-fp}} \\ u_{yq\text{-fp}} \end{bmatrix} = \begin{bmatrix} l\mathrm{p} + r & -l\omega_\mathrm{p} \\ l\omega_\mathrm{p} & l\mathrm{p} + r \end{bmatrix} \begin{bmatrix} i_{pd\text{-fp}} \\ i_{pq\text{-fp}} \end{bmatrix} \\
\qquad\qquad - (D_\mathrm{p} - 1) B_\mathrm{p}' \begin{bmatrix} u_{pd} \\ u_{pq} \end{bmatrix} \\
(D_\mathrm{s} - 1) \begin{bmatrix} u_{yd\text{-fs}} \\ u_{yq\text{-fs}} \end{bmatrix} = \begin{bmatrix} l\mathrm{p} + r & -l\omega_\mathrm{s} \\ l\omega_\mathrm{s} & l\mathrm{p} + r \end{bmatrix} \begin{bmatrix} i_{sd\text{-fs}} \\ i_{sq\text{-fs}} \end{bmatrix} \\
\qquad\qquad + (D_\mathrm{s} - 1) \begin{bmatrix} u_{sd} \\ u_{sq} \end{bmatrix}
\end{cases}
\tag{16}
$$

III. CONTROL SCHEME

An overview of the control scheme of Hexverter is presented in Fig. 3, which realizes flexible active/reactive power control on both sides and achieves overall stability of the stored energy. It is characterized by a structure consisting of the following three blocks:

- Outer-loop voltage control block.
- Inner-loop current control block.
- The branch voltage-balancing control block

A. OUTER-LOOP VOLTAGE CONTROL

Fig. 3 shows the outer-loop voltage control, which controls the stored energy of the Hexverter. The outer-loop voltage control achieved overall stability of the stored energy. P_s and P_s^* are the actual and set values of the active power of the secondary side system, respectively. Q_s and Q_s^* are the actual and set values, respectively, of the reactive power of the secondary side system. $u_{\text{dc-av}}$ and $u_{\text{dc-av}}^*$ are the actual and set values, respectively, for the average DC voltage of all submodules in Hexverter. Q_p and Q_p^* are the actual and set values of the reactive power of the primary-side system, respectively.

B. INNER-LOOP CURRENT CONTROL

Fig. 3 shows the inner-loop current control, which can be derived from (16). Based on the power control model, the inner loop current control realizes independent control of the decoupled AC voltages and currents, and achieves flexible

active/reactive power control on both sides of the AC system. In Fig. 3, the six-branch reference voltages in *dq* coordinates are $\{u_{xd\text{-fp}}, u_{xq\text{-fp}}\}$, $\{u_{xd\text{-fs}}, u_{xq\text{-fs}}\}$, $\{u_{yd\text{-fp}}, u_{yq\text{-fp}}\}$, and $\{u_{yd\text{-fs}}, u_{yq\text{-fs}}\}$.

C. THE BRANCH VOLTAGE-BALANCING CONTROL

The branch voltage-balancing control is a key problem for Hexverter. A branch voltage-balancing control model is proposed in this section.

1) THE ZERO-SEQUENCE NETWORK

The zero-sequence network is shown in Fig. 4. The zero-sequence voltages of the primary and secondary AC systems are represented by u_{p0} and u_{s0}, respectively, and the zero-sequence currents are represented by i_{p0} and i_{s0}, respectively. The submodules in each branch are replaced by a variable zero-sequence voltage source u_{j0} with $j \in \{1, 2, 3, 4, 5, 6\}$ in series with zero-sequence impedance r. The branch zero-sequence currents are i_{j0} with $j \in \{1, 2, 3, 4, 5, 6\}$.

The zero-sequence double-loop network is shown in Fig. 5. The zero-sequence circulating current has two loops. One is defined as the zero-sequence Y-loop circulating current that flows through the neutral point of the primary and secondary sides (as shown in Fig. 5(a), where the solid arrow lines represent one of the phases). The other is defined as the zero-sequence Hex-loop circulating current that flows through the six branches of Hexverter (as shown in Fig. 5(b)). The zero-sequence circulating currents in the branches include the Y-loop and Hex-loop circulating currents, which can be analyzed and controlled independently.

2) THE Y-LOOP CIRCULATING CURRENT MODEL

The zero-sequence Y-loop circulating current is illustrated in Fig. 5(a). Applying Kirchhoff's voltage and current laws to Fig. 5(a) yields:

$$
\begin{cases}
0 = u_{\mathrm{nN}} - u_{p0} - ri_{x0} + u_{x0} + u_{s0} \\
0 = u_{\mathrm{nN}} - u_{p0} + ri_{y0} - u_{y0} + u_{s0} \\
i_{p0} = -i_{x0} + i_{y0} \\
i_{s0} = +i_{x0} - i_{y0} \\
i_{p0} = -i_{s0} \\
u_{p0} = u_{s0} = 0
\end{cases}
\tag{17}
$$

where u_{x0} and i_{x0} are the zero-sequence voltages and currents of the branches $\{1, 3, 5\}$ respectively, and u_{y0} and i_{y0} are the zero-sequence voltages and currents of branches $\{2, 4, 6\}$, respectively.

From (17), the Y-loop circulating current is:

$$
i_{p0} = -i_{s0} = -\frac{u_{\mathrm{nN}}}{r} - \frac{u_{x0} - u_{y0} + ri_{x0} - ri_{y0}}{2r}
\tag{18}
$$

According to (18), the Y-loop circulating current can be suppressed to zero by setting the value of u_{nN} as

$$
u_{\mathrm{nN}} = -\frac{u_{x0} - u_{y0} + ri_{x0} - ri_{y0}}{2}
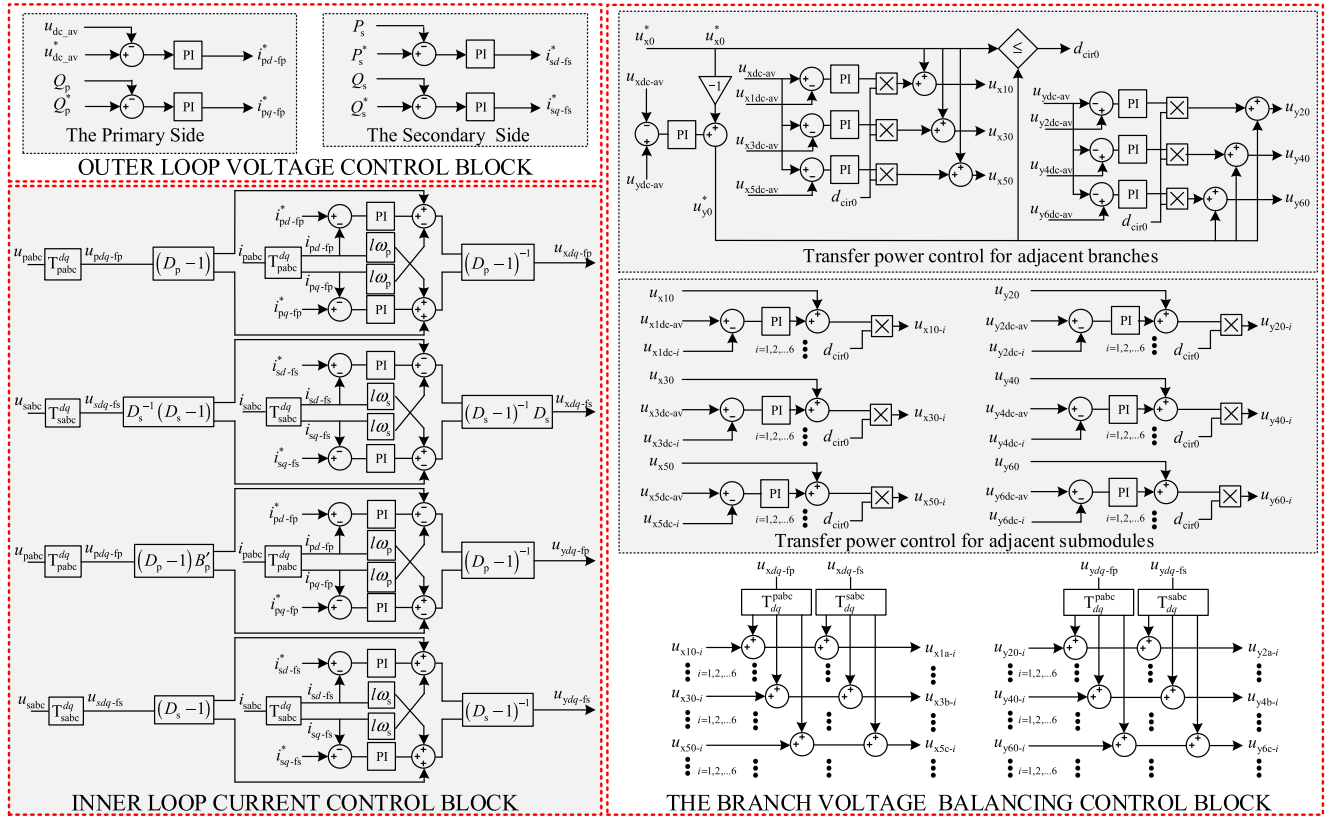\tag{19}
$$

FIGURE 3. Overview of control scheme of the Hexverter.

This paper proposes a novel grounding method for suppressing the Y-loop circulating current by connecting a capacitor at the neutral point. A neutral-point capacitor can be charged or discharged using a Y-loop circulating current. By regulating capacitor voltage u_{nN} to satisfy (19), the Y-loop circulating currents i_{p0} and i_{s0} can be suppressed. And then,

$$u_{nN} = -\frac{u_{x0} - u_{y0}}{2} \qquad (20)$$

3) THE TRANSFER POWER MODEL

The branch power differs ΔP between adjacent branches depending on the difference between the reactive powers in both AC systems [6]:

$$\Delta P = \frac{\sqrt{3}}{18}(Q_p - Q_s) \qquad (21)$$

The branch power differs leads to an imbalance of the submodule DC-links and further results in system breakdown or insufficient branch voltage reserves for the control system. When the difference between the reactive powers in both systems reaches the maximum value, the branch power differs ΔP and reaches its maximum value (ΔP_{max}). ΔP is a key problem for the Hexverter control to compensate for the difference in branch power. To solve this key problem, this study proposes a transfer power model based on the Hex-loop circulating current.
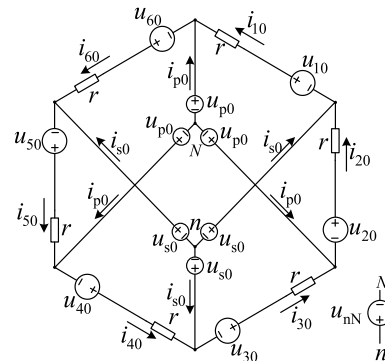

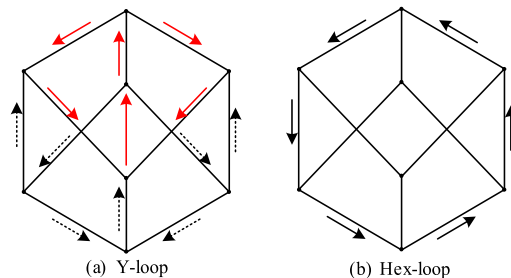**FIGURE 4.** The zero-sequence network.

(a) Y-loop (b) Hex-loop

FIGURE 5. The zero-sequence double-loop network.

Assuming that the zero-sequence Y-loop circulating current is suppressed to zero, the zero-sequence Hex-loop circulating current i_{cir0} is as shown in Fig. 5(b) and

can be expressed as

$$i_{\text{cir0}} = \sum_{i=1}^{6} u_{i0} \Bigg/ 6r = \frac{u_{x0} + u_{y0}}{2r} \qquad (22)$$

Mode A: If u_{x0} is set to a constant value, then the transfer power ΔP_{adj} is.

$$\Delta P_{\text{adj}} = i_{\text{cir0}} u_{x0} = \frac{u_{x0} + u_{y0}}{2r} u_{x0} \qquad (23)$$

where $u_{x0} < -\sqrt{2r\,|\Delta P_{\max}|}$ or $u_{x0} > \sqrt{2r\,|\Delta P_{\max}|}$.

Thus u_{y0} can be expressed as:

$$u_{y0} = \frac{2r\Delta P_{\text{adj}}}{u_{x0}} - u_{x0} \qquad (24)$$

And then:

$$u_{nN} = +\frac{r\Delta P_{\text{adj}}}{u_{x0}} - u_{x0} \qquad (25)$$

Mode B: If u_{y0} is set to a constant value, then the transfer power ΔP_{adj} is.

$$\Delta P_{\text{adj}} = i_{\text{cir0}} u_{y0} = -\frac{u_{x0} + u_{y0}}{2r} u_{y0} \qquad (26)$$

where $u_{y0} < -\sqrt{2r\,|\Delta P_{\max}|}$ or $u_{y0} > \sqrt{2r\,|\Delta P_{\max}|}$.

Thus u_{x0} can be expressed as:

$$u_{x0} = \frac{2r\Delta P_{\text{adj}}}{u_{y0}} - u_{y0} \qquad (27)$$

And then:

$$u_{nN} = +u_{y0} - \frac{r\Delta P_{\text{adj}}}{u_{y0}} \qquad (28)$$

According to (22)–(28), the values of $\{u_{x0}, u_{y0}\}$ determine the zero-sequence Hex-loop circulating current i_{cir0} and transfer power ΔP_{adj}. The relationships between i_{cir0}, ΔP_{adj}, and $\{u_{x0}, u_{y0}\}$ are listed in Table. 1.

The relationship between $\{u_{x0}, u_{y0}\}$ and the transfer power ΔP_{adj} is shown in Fig. 6. For example, as shown in Fig. 6(a), assuming u_{x0} is fixed at -0.05pu, ΔP_{adj} is regulated as u_{y0} changes in work area A.

In addition, the relationship between the zero-sequence voltage $\{|u_{x0}|, |u_{y0}|\}$, the Hex-loop circulating current i_{cir0}, and the neutral point u_{nN} can be analyzed using (20), (22), (25), and (28). According to (20), the larger the zero-sequence voltage $\{|u_{x0}|, |u_{y0}|\}$, the larger is the neutral point u_{nN}. According to (22), (25), and (28), the larger the zero-sequence voltage $\{|u_{x0}|, |u_{y0}|\}$, the smaller is the Hex-loop circulating current i_{cir0}. Therefore, under the constraint of the neutral-point DC bias voltage, a larger $\{|u_{x0}|, |u_{y0}|\}$ should be set as much as possible to suppress the Hex-loop circulating current.

According to the transfer power model, the branch energy can be directly regulated among its adjacent submodules and branches by the zero-sequence Hex-loop circulating current.

TABLE 1. The relationships between ΔP_{adj}, i_{cir0}, and u_{x0}, u_{y0}.

THE VALUES OF $\{u_{x0}, u_{y0}\}$		direction of i_{cir0} $\{d_{\text{cir0}}\}$	ΔP_{adj}
If $u_{x0}+u_{y0}>0$	when $u_{x0}>0$, $u_{y0}>0$	$i_{\text{cir0}}>0$	$\times$ [1]
	when $u_{x0}>0$, $u_{y0}<0$		$\Delta P_{\text{adj}}>0$ [2]
	when $u_{x0}<0$, $u_{y0}>0$		$\Delta P_{\text{adj}}<0$ [3]
If $u_{x0}+u_{y0}=0$	when $u_{x0}>0$, $u_{y0}<0$	$i_{\text{cir0}}=0$	$\times$
	when $u_{x0}<0$, $u_{\,0}>0$		
If $u_{x0}+u_{y0}<0$	when $u_{x0}<0$, $u_{y0}<0$	$i_{\text{cir0}}<0$	$\times$
	when $u_{x0}>0$, $u_{y0}<0$		$\Delta P_{\text{adj}}<0$
	when $u_{x0}<0$, $u_{y0}>0$		$\Delta P_{\text{adj}}>0$

[1] $\times$ indicates that the system cannot be stable.
[2] $\Delta P_{\text{adj}}>0$: branch$\{1,3,5\}$ are discharged, and branch$\{2,4,6\}$ are charged.
[3] $\Delta P_{\text{adj}}<0$: branch$\{1,3,5\}$ are charged, and branch$\{2,4,6\}$ are discharged.

4) THE BRANCH VOLTAGE-BALANCING CONTROL

The branch voltage-balancing control is proposed in this section. The magnitude and direction of the transfer power ΔP_{adj} among the submodules can be regulated by dynamically adjusting the zero-sequence voltages of each submodule. The zero-sequence voltages of each submodule can determine the charging or discharging states of the corresponding submodules, and the steady-state balance of the branch voltages is achieved. The transfer power control consists of two control processes.
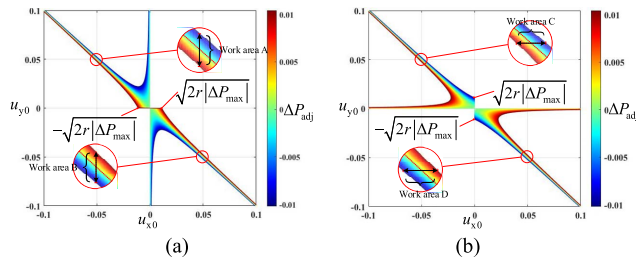
- Transfer power control of adjacent branches

According to the transfer power model established above, the transfer power ΔP_{adj} between the adjacent branches can be regulated by controlling $\{u_{x0}, u_{y0}\}$. The transfer power ΔP_{adj} is the key to compensating for the difference in the active power ΔP between the adjacent branches. Fig. 3 shows the transfer power control of the adjacent branches. $u_{\text{xdc-av}}$ and $u_{\text{ydc-av}}$ are the actual values for the average DC voltage of all the submodules in branches $\{1, 3, 5\}$ and $\{2, 4, 6\}$, respectively. u_{x10}, u_{x30}, u_{x50} and u_{y20}, u_{y40}, u_{y60} are the zero-sequence voltages of branches $\{1, 3, 5\}$ and $\{2, 4, 6\}$, respectively.

- Transfer power control of adjacent submodules

Based on the transfer power model, the transfer power ΔP_{adj} between adjacent submodules can be regulated by controlling the zero-sequence voltages of each submodule. Fig. 3 shows the transfer power control of the adjacent submodules in the branches. $u_{x10\text{-}i}$, $u_{x30\text{-}i}$, $u_{x50\text{-}i}$ and $u_{y20\text{-}i}$, $u_{y40\text{-}i}$, $u_{y60\text{-}i}$ $(i = 1, 2, \ldots n)$ are the zero-sequence voltages of submodules i in branches $\{1, 3, 5\}$ and $\{2, 4, 6\}$, respectively. The number of submodules per branch is n. The reference voltages of each submodule are $\{u_{x1a\text{-}i}, u_{x3b\text{-}i}, u_{x5c\text{-}i}\}$ and $\{u_{y2a\text{-}i}, u_{y4b\text{-}i}, u_{y6c\text{-}i}\}$ and can be calculated using $\{u_{x10\text{-}i}, u_{x30\text{-}i}, u_{x50\text{-}i}\}$ and $\{u_{y20\text{-}i}, u_{y40\text{-}i}, u_{y60\text{-}i}\}$ $(i = 1, 2, \ldots n)$, $\{u_{xd\text{-fp}}, u_{xq\text{-fp}}\}$, $\{u_{xd\text{-fs}}, u_{xq\text{-fs}}\}$, $\{u_{yd\text{-fp}}, u_{yq\text{-fp}}\}$, and $\{u_{yd\text{-fs}}, u_{yq\text{-fs}}\}$.

D. THE BENEFITS OF THE PROPOSED CONTROL STRATEGY

The branch voltage-balancing control model proposed in this study is based on a zero-sequence network, whereas the

FIGURE 6. The relationship between {u_{x0}, u_{y0}} and the transfer power ΔP_{adj}: (a) mode A; (b) mode B.

ITEMS	PARAMETERS	VALUE
Hexverter	Number of submodules per branch	6
	Submodule capacitance	10mF
	Branch inductance	1mH
	Branch resistance	0.08Ω
	Neutral-point capacitance	10nF
	Nominal Submodule DC voltage	4000V
	Nominal Power	20MVA
The primary side AC system	Frequency	50Hz
	Line voltage RMS	10.5kV
The secondary side AC system	Frequency	60Hz
	Line voltage RMS	11.4kV

power control model is based on a positive-sequence network. The relative independence of the positive- and zero-sequence networks leads to decoupling of the branch voltage balance control model and the power control model, and the respective control objectives can be achieved by adjusting the decoupled control variables. Therefore, the control parameters of the two controllers can be adjusted independently, which is beneficial for the design and optimization of the control parameters.

IV. SIMULATION RESULTS

A. SIMULATION PARAMETERS

Simulation is performed to verify the operating principle of the Hexverter in Fig.1 which is built in MATLAB/Simulink software. The key simulation parameters of Hexverter are listed in Table 2.

B. THE STEADY AND TRANSIENT STATE SIMULATION

To verify the steady and transient performances of the control scheme mentioned earlier, a series of step changes were set during the simulation process. The steady and transient performances of Hexverter under balanced and unbalanced grid conditions are investigated and compared in Fig. 7 and Fig. 8, respectively.

The corresponding simulation waveforms under the balanced grid conditions are shown in Fig. 7. Fig. 7(a) and (c) show the AC voltages of the two sides of Hexverter, respectively. Fig. 7(b) and (d) show the AC currents of two sides of Hexverter, respectively. The branch voltages are multilevel, as shown in Fig. 7(e) and (f). Fig. 7(g) shows the average DC voltages of all submodules. Under balanced grid conditions, the currents exhibit the same changing tendency during step changes, and the average DC voltage is maintained at the rated value with a slight fluctuation after step changes.

The corresponding simulation waveforms under the unbalanced grid conditions are shown in Fig. 8. Fig. 8(a) and (c) show the AC voltages at the two sides of Hexverter, respectively. Fig. 8(b) and (d) show the AC currents at two sides of Hexverter, respectively. The branch voltages are multilevel, as shown in Fig. 8(e) and (f). Fig. 8(g) shows the average DC voltages of all submodules. Under unbalanced grid conditions, the currents remain balanced and have the same changing tendency during step changes, and the average

DC voltage is maintained at the rated value with a slight fluctuation after step changes.

The corresponding simulation waveforms under variations in the frequency of the AC system are shown in Fig. 9. Fig. 9(a) and (c) show the AC voltages at the two sides of Hexverter, respectively. Fig. 9(b) and (d) show the AC currents at two sides of Hexverter, respectively. The branch voltages are multilevel, as shown in Fig. 9(e) and (f). Fig. 9(g) shows the average DC voltages of all submodules. After the step change in the frequency of the secondary-side AC system, the secondary current remained balanced and rated. The primary current returned to the rated value after a brief transition. The average DC voltage was maintained at the rated value with slight fluctuation.

The corresponding simulation waveforms under variations in the frequency of the AC system are shown in Fig. 10. Fig. 10(a) and (c) show the AC voltages at the two sides of Hexverter, respectively. Fig. 10(b) and (d) show the AC currents at two sides of Hexverter, respectively. The branch voltages are multilevel, as shown in Fig. 10(e) and (f). Fig. 10(g) shows the changes in the frequency of the secondary-side AC system. Fig. 10(h) shows the average DC voltages of all submodules. Along with changes in the frequency of the secondary-side AC system, the primary and secondary currents remain balanced and rated. The average DC voltage was maintained at the rated value with slight fluctuation.

The simulation results confirmed that the designed control scheme can adapt well to the asymmetry of the grid, has superior steady-state performance under both balanced and unbalanced grid conditions, and exhibits good control characteristics in transient operations. The control strategy proposed in this study has stronger adaptability to diverse power grid operating parameters.

C. THE BRANCH VOLTAGE-BALANCING CONTROL

The following comparative simulations were performed to verify The branch voltage-balancing control on the energy imbalance of the submodule DC links. To make the waveform differences more identifiable, significant asymmetrical
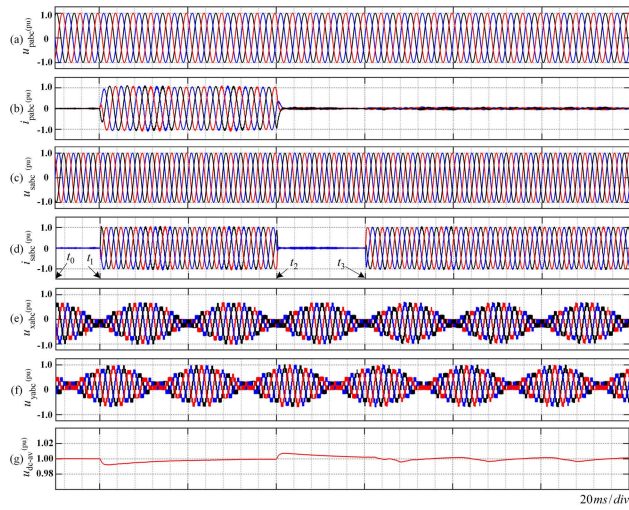
FIGURE 7. Steady and transient performances of the control scheme under balanced grid conditions. The step changes: 1) The active power of the secondary side steps from 0.0pu to 1.0pu at t_1; 2) The active power of the secondary side steps from 1.0pu to 0.0pu at t_2; 3) The reactive power of the secondary side steps from 0.0pu to 1.0pu at t_3, and the reactive power of the primary side remains at 0.0pu. All waveforms are in pu.
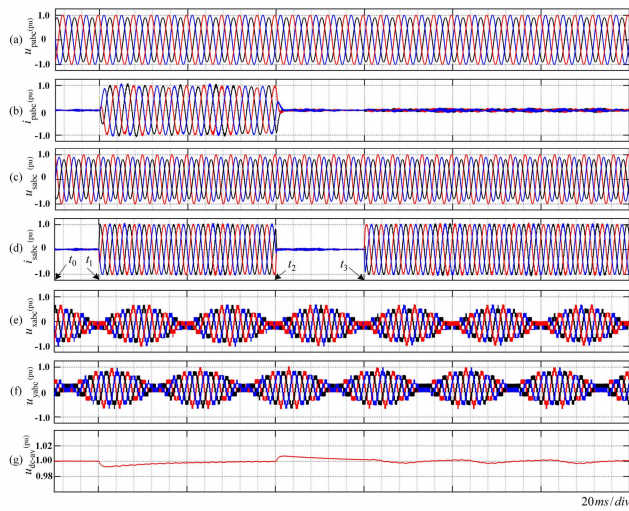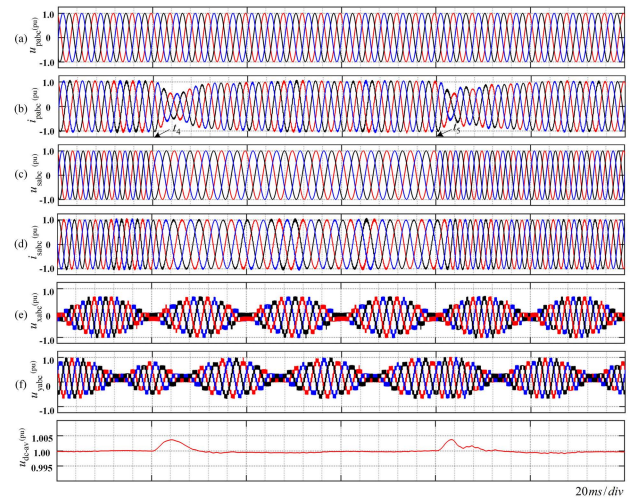

FIGURE 8. Steady and transient performances of the control scheme under unbalanced grid conditions. The unbalanced grid parameters: $u_{pc} = 0.9$pu, $u_{sb} = 0.9$pu, $u_{sc} = 0.8$pu.The step changes: 1) The active power of the secondary side P_S steps from 0.0pu to 1.0pu at t_1; 2) The active power of the secondary side steps from 1.0pu to 0.0pu at t_2; 3) The reactive power of the secondary side Q_S steps from 0.0pu to 1.0pu at t_3, and the reactive power of the primary side Q_P remains at 0.0pu.

FIGURE 9. Steady and transient performances of the control scheme under variations in the frequency of the AC system. Parameters: $P_S = 1.0$pu, $Q_S = 0$pu, $Q_P = 0$pu, $f_P = 50$Hz. f_S steps from 60 Hz to 40 Hz at t_4 and step back to 60 Hz at t_5.

FIGURE 10. Steady and transient performances of the control scheme under variations in the frequency of the AC system. Parameters $P_S = 1.0$pu, $Q_S = 0$pu, $Q_P = 0$pu, $f_P = 50$ Hz, and f_S changes from 60 Hz to 35 Hz during t_6 and t_7.
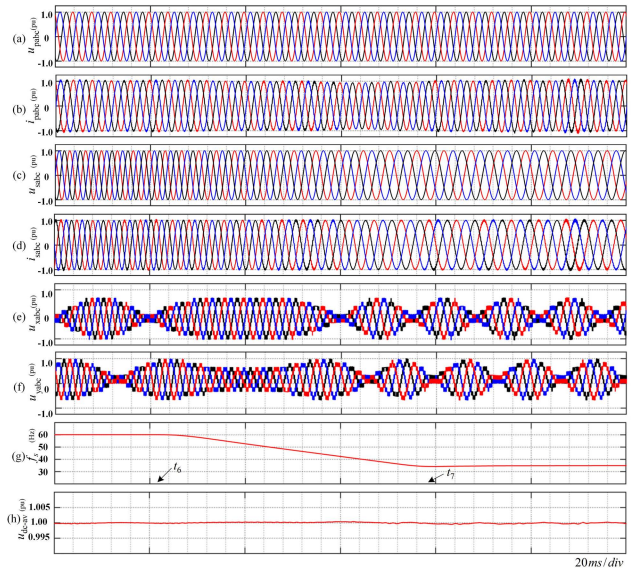
parameters were set in the DC link of each submodule in the simulation.

The corresponding simulation waveforms are shown in Fig. 11. Fig. 11(a) shows the average DC voltages of all submodules. Fig. 11(b) shows the average DC voltages of the submodules in branches {1, 3, 5} and {2, 4, 6}. The six DC voltages of the submodules in branches {5, 6} are plotted in the graphs shown in Fig. 11(c) and (d), respectively. The corresponding zero-sequence voltages are plotted in each graph shown in Fig. 11(e) and (f), respectively.

Based on the outer-loop voltage control, the average DC voltage of all submodules is kept at 1.0pu, as shown in

Fig. 11(a). Because of the asymmetrical parameters of the submodules and branches, the average DC voltages {$u_{xdc\text{-}av}$, $u_{ydc\text{-}av}$} and the corresponding DC voltages {$u_{x5dc\text{-}i}$, $u_{y6dc\text{-}i}$} ($i = 1, 2, \ldots, 6$) in branches {5, 6} begin to diverge significantly, as shown in Fig. 11(b), (c), and (d).

After applying the proposed branch voltage-balancing control at t_8, the zero-sequence voltages {$u_{x10\text{-}i}$, $u_{x30\text{-}i}$, $u_{x50\text{-}i}$} and {$u_{y20\text{-}i}$, $u_{y40\text{-}i}$, $u_{y60\text{-}i}$} were superimposed onto the reference voltages of each submodule. The zero-sequence voltages {$u_{x50\text{-}i}$, $u_{y60\text{-}i}$} ($i = 1, 2, \ldots, 6$) of the submodules in branches {5,6} are shown in Fig. 11(e) and (f). Based on the transfer power model, the transfer power ΔP_{adj} can be regulated by zero-sequence voltages {$u_{x10\text{-}i}$, $u_{x30\text{-}i}$, $u_{x50\text{-}i}$} and {$u_{y20\text{-}i}$, $u_{y40\text{-}i}$, $u_{y60\text{-}i}$}. Submodules with higher DC voltages
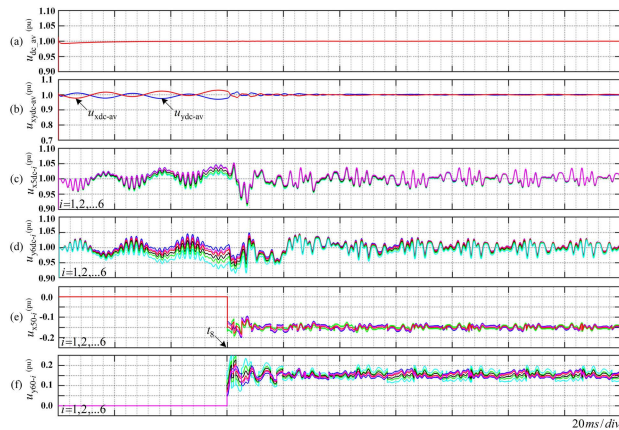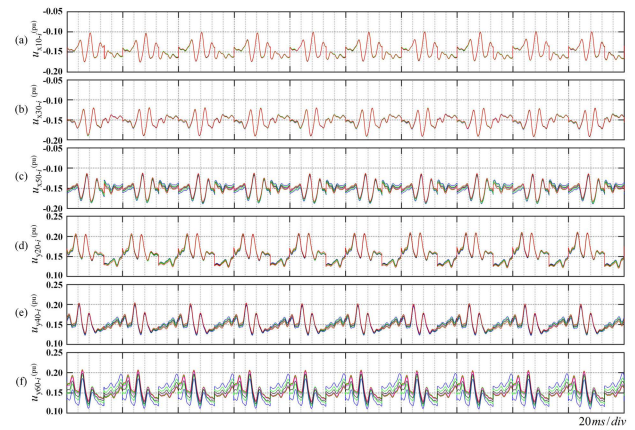
FIGURE 11. Performance of The branch voltage-balancing control. Parameters: $P_s = 1.0pu$, $Q_s = 0pu$, $Q_p = 0pu$. The branch voltage-balancing control is applied at t_8.

FIGURE 12. Waveforms of the zero-sequence voltages of all submodules under The branch voltage-balancing control. Parameters: $P_s = 0pu$, $Q_s \neq Q_p$, $Q_s = 1.0pu$, $Q_p = 0pu$.

FIGURE 13. Waveforms of the DC voltages of all submodules under The branch voltage-balancing control. Parameters: $P_s = 0pu$, $Q_s \neq Q_p$, $Q_s = 1.0pu$, $Q_p = 0pu$.

are discharged, whereas submodules with lower DC voltages are charged. The corresponding average DC voltages $\{u_{xdc\text{-}av}, u_{ydc\text{-}av}\}$ and the DC voltages of each submodule were merged to the rated value and maintained at a constant value with slight fluctuations. The waveforms of the voltages $\{u_{xdc\text{-}av}, u_{ydc\text{-}av}\}$ and $\{u_{x5dc\text{-}i}, u_{y6dc\text{-}i}\}$ $(i = 1, 2, \ldots, 6)$ are shown in Fig. 11(b), (c), and (d). This indicates the effectiveness of the proposed The branch voltage-balancing control.

The zero-sequence voltages $\{u_{x10\text{-}i}, u_{x30\text{-}i}, u_{y20\text{-}i}, u_{y40\text{-}i}\}$ are similar to $\{u_{x50\text{-}i}, u_{y60\text{-}i}\}$, and the corresponding DC voltages $\{u_{x1dc\text{-}i}, u_{x3dc\text{-}i}, u_{y2dc\text{-}i}, u_{y4dc\text{-}i}\}$ are also similar to $\{u_{x5dc\text{-}i}, u_{y6dc\text{-}i}\}$ and thus are not shown for simplicity.

The following simulations were performed to verify the effectiveness of the proposed control strategy under typical operating conditions: The active and reactive powers of the secondary side of Hexverter were 0pu and 1.0pu, respectively. The reactive power on the primary side was 0pu. Because of the asymmetry of the reactive power on both sides $Q_s \neq Q_p$, the branch power differs between adjacent branches. To make the waveform differences more identifiable, significant asymmetrical parameters were set in the DC link of each submodule in the simulation.

The corresponding simulation waveforms are shown in Fig. 12 and Fig. 13, respectively. The six zero-sequence voltages and six DC voltages of the submodules in each branch are plotted in each graph in Fig. 12 and Fig. 13, respectively. Owing to the asymmetrical parameters in the DC-link of submodules and the branch power differs between adjacent branches, more complex transfer power values for each submodule are required to achieve a DC voltage balance. The more unbalanced the submodule parameters, the greater the required transfer power, and the more significant the difference between the zero-sequence voltages of the corresponding submodules, as shown in Fig. 12. The submodules in branch {6} have the most severe asymmetrical parameters; therefore, the differences in the zero-sequence voltages of its submodules are significant, as shown in Fig. 12(f). Under The branch voltage-balancing control, the DC voltages of each submodule are maintained at a constant value with
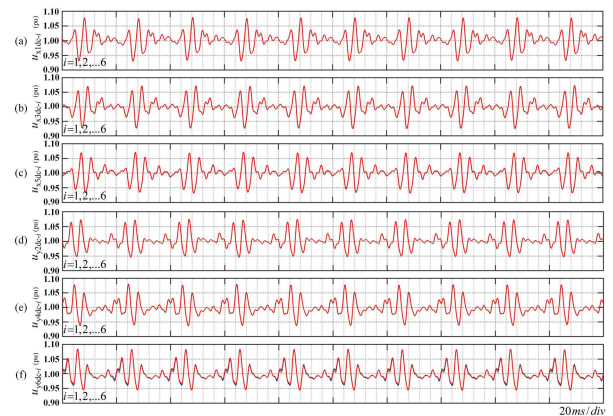
slight fluctuations, and there are only minor differences in the six DC voltages in each branch, as shown in Fig. 13. This indicates the effectiveness of the proposed branch voltage-balancing control.

V. CONCLUSION

In summary, a novel branch voltage-balancing control strategy is proposed in this study. An active and reactive power control model based on a double-*dq* transformation was proposed. It realizes flexible active/reactive power control on both sides and achieves overall stability of the stored energy. This study establishes a novel branch voltage-balancing control strategy based on a transfer power model. The essence of the proposed control strategy is to control the charging and discharging states of each submodule via the zero-sequence voltages and Hex-loop circulating current to regulate the power transfer between adjacent submodules and branches and effectively ensure the dynamic balance of the DC voltages of the submodules. The branch voltage-balancing control model and power control model proposed in this paper are based on zero-sequence and positive-sequence networks, respectively. The relative independence of the positive- and

zero-sequence networks leads to decoupling of the branch voltage balance control model and the power control model; thus, the respective control objectives can be achieved by adjusting the respective control variables independently. It has a stronger adaptability to diverse power grid operating parameters. Finally, the validity and correctness of the mathematical model and control strategy proposed in this study were verified through a series of simulations based on MATLAB/Simulink.

REFERENCES

[1] M. Glinka and R. Marquardt, "A new AC/AC multilevel converter family," *IEEE Trans. Ind. Electron.*, vol. 52, no. 3, pp. 662–669, Jun. 2005.

[2] T. Friedli, J. W. Kolar, J. Rodriguez, and P. W. Wheeler, "Comparative evaluation of three-phase AC–AC matrix converter and voltage DC-link back-to-back converter systems," *IEEE Trans. Ind. Electron.*, vol. 59, no. 12, pp. 4487–4510, Dec. 2012.

[3] R. W. Erickson and O. A. Al-Naseem, "A new family of matrix converters," in *Proc. 27th Annu. Conf. IEEE Ind. Electron. Soc. (IECON)*, 2001, pp. 1515–1520.

[4] W. Kawamura, M. Hagiwara, and H. Akagi, "Control and experiment of a modular multilevel cascade converter based on triple-star bridge cells," *IEEE Trans. Ind. Appl.*, vol. 50, no. 5, pp. 3536–3548, Sep./Oct. 2014.

[5] B. Fan, K. Wang, Z. Zheng, L. Xu, and Y. Li, "Optimized branch current control of modular multilevel matrix converters under branch fault conditions," *IEEE Trans. Power Electron.*, vol. 33, no. 6, pp. 4578–4583, Jun. 2018.

[6] L. Baruschka and A. Mertens, "A new three-phase AC/AC modular multilevel converter with six branches in hexagonal configuration," *IEEE Trans. Ind. Appl.*, vol. 49, no. 3, pp. 1400–1410, May 2013.

[7] L. Baruschka and A. Mertens, "A new 3-phase direct modular multilevel converter," in *Proc. 14th Eur. Conf. Power Electron. Appl.*, Aug./Sep. 2011, pp. 1–10.

[8] G. Lambert, A. Costabeber, P. Wheeler, and Y. R. De Novaes, "A unidirectional insulated AC–DC converter based on the hexverter and multipulse-rectifier," *IEEE Trans. Power Electron.*, vol. 35, no. 3, pp. 2363–2371, Mar. 2020.

[9] H. R. Robles-Campos and F. Mancilla-David, "A control scheme in the dq reference frame for hexverter-based systems," in *Proc. North Amer. Power Symp. (NAPS)*, Oct. 2019, pp. 1–6.

[10] C. Zhang, D. Jiang, X. Zhang, J. Chen, C. Ruan, and Y. Liang, "The study of a battery energy storage system based on the hexagonal modular multilevel direct AC/AC converter (Hexverter)," *IEEE Access*, vol. 6, pp. 43343–43355, 2018.

[11] Y. Meng, Y. Zou, H. Li, J. Yu, and X. Wang, "A global asymptotical stable control scheme for a hexverter in fractional frequency transmission systems," *J. Mod. Power Syst. Clean Energy*, vol. 7, no. 6, pp. 1495–1506, Nov. 2019.

[12] D. Karwatzki, L. Baruschka, M. von Hofen, and A. Mertens, "Branch energy control for the modular multilevel direct converter hexverter," in *Proc. IEEE Energy Convers. Congr. Expo. (ECCE)*, Sep. 2014, pp. 1613–1622.

[13] D. Karwatzki and A. Mertens, "Generalized control approach for a class of modular multilevel converter topologies," *IEEE Trans. Power Electron.*, vol. 33, no. 4, pp. 2888–2900, Apr. 2018.

[14] Y. Meng, B. Liu, H. Luo, S. Shang, H. Zhang, and X. Wang, "Control scheme of hexagonal modular multilevel direct converter for offshore wind power integration via fractional frequency transmission system," *J. Mod. Power Syst. Clean Energy*, vol. 6, no. 1, pp. 168–180, Jan. 2018.

[15] Y. Yi, C. Qian, Y. Gui, and G. Yang, "Circulating current suppressing strategy based on zero-sequence network model for hexverter," in *Proc. IEEE 3rd Int. Conf. Circuits Syst. (ICCS)*, Oct. 2021, pp. 256–266.

YANG YI was born in Leping, Jiangxi, China, in 1984. He received the B.S., M.S., and Ph.D. degrees from the Department of Electrical Engineering, Huazhong University of Science and Technology (HUST), Hubei, China, in 2007, 2009, and 2013, respectively. From 2013 to 2019, he was a Senior Engineer at State Grid Fujian Electric Power Company, China. In 2019, he joined Fuzhou University (FZU). He is currently an Associate Professor at FZU. His research interests include power system operation, control, and applications of high-power electronic technology in power systems.

GANG YANG was born in Xinchang, Zhejiang, China, in 1997. He received the B.S. degree from the College of Electrical Engineering and Automation, Fuzhou University, Fujian, China, where he is currently pursuing the M.S. degree.

CHONG QIAN was born in Fengxian, Jiangsu, China, in 1995. He received the B.S. degree from the Changzhou Institute of Technology, Jiangsu. He is currently pursuing the M.S. degree with the College of Electrical Engineering and Automation, Fuzhou University, Fujian, China.

YAOJIE GUI was born in Xuanhan, Sichuan, China, in 1998. He received the B.S. degree from the Sichuan University of Science & Engineering, Sichuan. He is currently pursuing the M.S. degree with the College of Electrical Engineering and Automation, Fuzhou University, Fujian, China.

• • •